ACS OMEGA

Open Access

http://pubs.acs.org/journal/acsodf

Article

Microwave Reactor with Combined Rigid and Flexible Stirring Paddles for Improving Fluid Heating Uniformity in Soft Manganese Ore Leaching Processes

Shujin Chen, Shaodou Cen, Renlong Liu,* Changyuan Tao, Shenghui Guo, and Guo Chen

Cite This: *ACS Omega* 2023, 8, 42367−42378

Read Online

ACCESS | Metrics & More | Article Recommendations

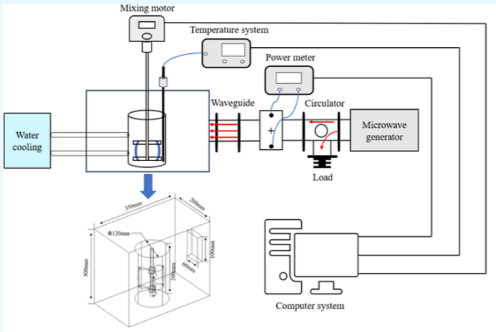

Schematic diagram of the experimental system

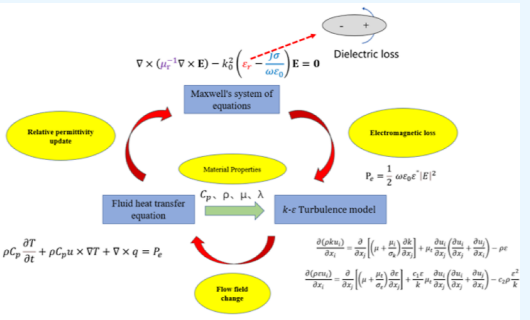

Flow chart of simulation calculation

ABSTRACT: In order to overcome the apparent limitations of the inhomogeneous nature of large-scale microwave heating of fluids, a microwave reactor with a rigid−flexible combined stirring paddle is used to heat fluids, destabilizing the hot spots present in the microwave heating of fluids process. An integrated multiphysics field simulation model for calculating the microwave heating process with fluid was created for the purpose of clarifying the temperature field dispersion and fluid flow patterns in the reactor. By using the proposed model, the rigid−flexible combined stirring paddle is compared with the conventional single- and double-layer stirring paddle to highlight the benefits of the rigid−flexible combined stirring paddle in improving fluid heating uniformity. It was found experimentally that the leaching rate of soft manganese ore was increased by 7.08 and 5.22% compared to conventional single and double stirred paddles, respectively. In addition, the optimal stirrer parameters were investigated by the response surface method.

1. INTRODUCTION

Manganese is an important strategic resource with irreplaceable application value in the national economy and steel industry.[1] With the development of social economy, the demand for manganese alloys is increasing, and it is especially important to recover manganese from the large amount of low-grade manganese ore, which accounts for about 93% of manganese resources.[2,3] There are two main methods of manganese resource recovery, pyrometallurgy and hydrometallurgy.[4] Although pyrometallurgy has a good recovery rate and higher efficiency, it has the disadvantage of high energy consumption and serious pollution in the recovery process.[5,6] In contrast, hydrometallurgy focuses on the recovery of low-grade minerals in a low-pollution manner.[7] In contrast, the conventional hydrometallurgical process has a low leaching rate and low economic efficiency. Therefore, the development of economical, clean, and efficient recovery technology for low-grade manganese ore is of great importance for the sustainable development of the manganese industry.

Microwave heating is fast, efficient, and has the advantage of selective heating,[8] therefore, microwave reactors are used in assisted chemical production.[9,10] It is used frequently as an alternative to conventional heating, especially in the fields of mineral pretreatment or reduction, ceramic or alloy material preparation.[5,11] Ye et al. conducted microwave carbon thermal reduction experiments on low-grade soft manganese ores and obtained a reduction rate of 97.2% at a shorter reduction time and lower processing temperature, 97.2% reduction was obtained.[12] However, the inhomogeneous electromagnetic field distribution present in the microwave heating process causes uncontrollable hot and cold spots with significant

Received: June 30, 2023
Accepted: October 9, 2023
Published: October 31, 2023

https://doi.org/10.1021/acsomega.3c04679
ACS Omega 2023, 8, 42367−42378

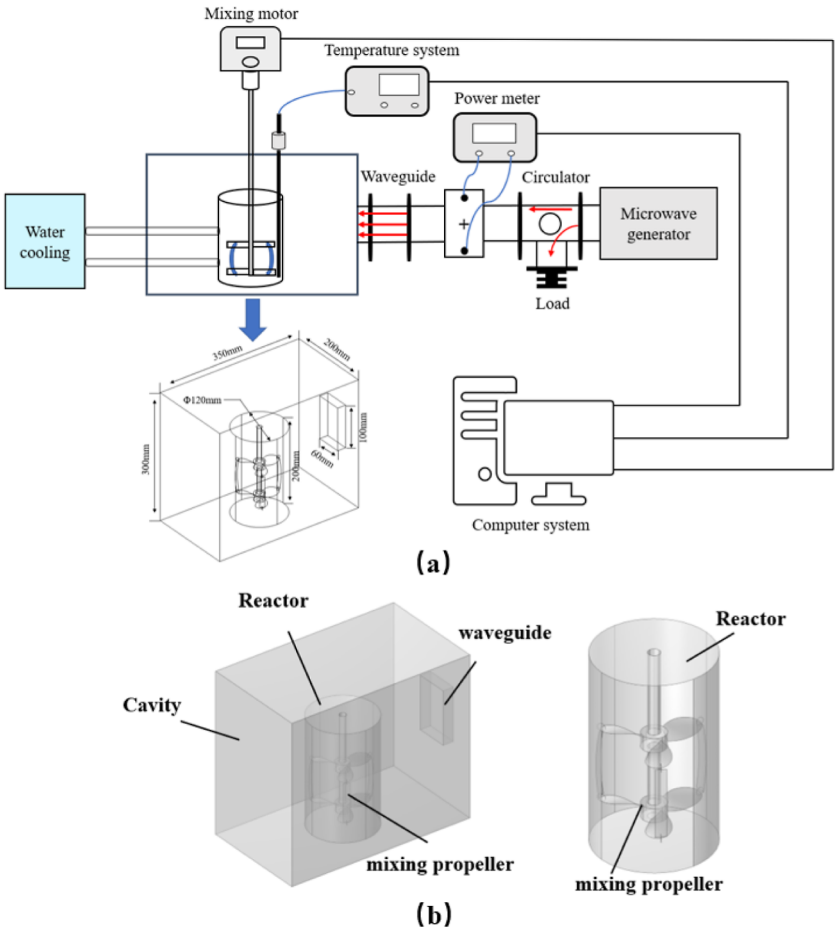

Figure 1. (a) Schematic diagram of the experimental system. (b) Schematic diagram of the 3D model.

heating inhomogeneity,[13] which limits the efficiency of microwave heating of chemical reactions.[14]

To solve this problem, various research methods have been proposed to improve the effect of microwave heating, including: modulating the electromagnetic field distribution in the microwave reactor, such as, by rotating a turntable with a metal patch to change the electromagnetic field distribution in the reactor, to improve the uniformity of microwave heating,[15] adding a mode stirrer in the microwave reactor is also beneficial to enhancing the microwave heating effect.[16] Through the turntable constantly altering the position of the reactants, so that the heat is evenly distributed, which improves the uniformity of microwave heating;[17] In besides varying the electromagnetic field distribution and changing the position of the reactants, the effect of microwave heating can be further enhanced by using fluid stirring technology, which greatly improves the heating uniformity compared to the case without stirring.[18]

For fluid heat transfer in a reactor, the fluid temperature distribution is constantly changed by the fluid flow. If the fluid is not in a laminar flow but in a turbulent state with a more complex fluid motion, the fluid temperature variation in the reactor will be more complex. Based on this situation, relevant numerical simulation studies of the fluid in the turbulent state of microwave reactor heating have not been reported. Nevertheless, in actual chemical production, high-speed stirring of the reactants is often required, and the designed reactor will be used in chemical production, for which simulation of the heating process is of great significance.

In our previous research, we designed a novel stirring paddle by combining rigid and flexible paddles to facilitate the adequate mixing of liquids in the reactor. Compared with the conventional rigid paddle, the combined rigid−flexible stirring paddle, subsequently referred to as RF stirring paddle, can effectively break the symmetric flow field and enhance the fluid flow inside the reactor.[19,20] Therefore, it can be expected that the added RF stirring paddle during microwave heating of the fluid will improve the temperature field distribution in the reactor and contribute to a more uniform distribution of the temperature field in the reactor. In this paper, by using the RF stirring paddle into the microwave reactor, the multiphysical field coupling calculation of electromagnetic field, temperature field, and flow field of the material inside the reactor was carried out to highlight the advantages of the RF stirring paddle to improve the microwave heating effect compared with the conventional paddle type. In addition, the microwave heating and fluid flow processes with different rotational speeds, off-bottom distances, rigid paddle diameters, and flexible paddle widths were calculated to determine their effects on the reactor temperature distribution, and the optimal stirring paddle parameters were determined by the response surface method.

2. METHODS

2.1. Experimental Section. In the experiment, first, the received soft manganese ore and pyrite were dried in an oven (Shanghai Yiheng Scientific Instruments Co., Ltd.) at 105 °C

https://doi.org/10.1021/acsomega.3c04679
ACS Omega 2023, 8, 42367−42378

Table 1. Summary of Material Properties of the Mineral Slurry in the Simulation

parameter	value	unit
the real part of the relative permittivity (ε')	$15.4251 + 0.0483 \times T$	dimensionless
the imaginary part of the relative permittivity (ε'')	$-0.49538 + 0.0037 \times T$	dimensionless
dynamic viscosity (μ)	$0.0003 + 17.7110 \times \exp(-T/29.205)$	Pa·s
thermal conductivity (K)	$-0.8691 + 0.0089 \times T^{1-1.5837\times10^{-5}} \times T^{2+7.9754\times10^{-9}} \times T^{3}$	W/(m^3·K)

for 2 h to remove any moisture that might have adhered to the surface. In the leaching experiment, soft manganese ore and pyrite with a 3:1 ratio of two ores were weighed by using an analytical scale (OHAUS). Then the required volume of sulfuric acid was added according to the liquid to solid ratio (10 mL/g). The microwave heating apparatus developed by Kunming University of Technology was used for microwave heating,[2] and the temperature of the solution in the reactor was measured in all experiments using a k-type digital temperature controller with a measurement range of 0−300 °C and a temperature accuracy of ±0.1 °C. The reaction time was controlled by a digital chronograph.[21] During the leaching process in the reactor, the sulfuric acid solution was stirred after a certain amount of the prepared sample was added, while

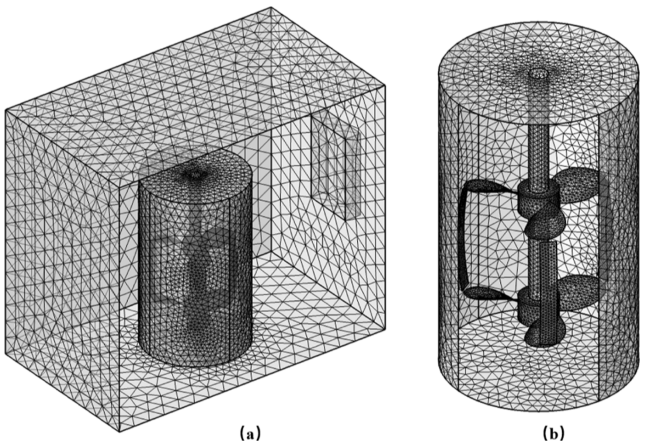

Figure 3. Meshing of (a) the general geometry and (b) the RF stirrer with tetrahedral mesh cells.

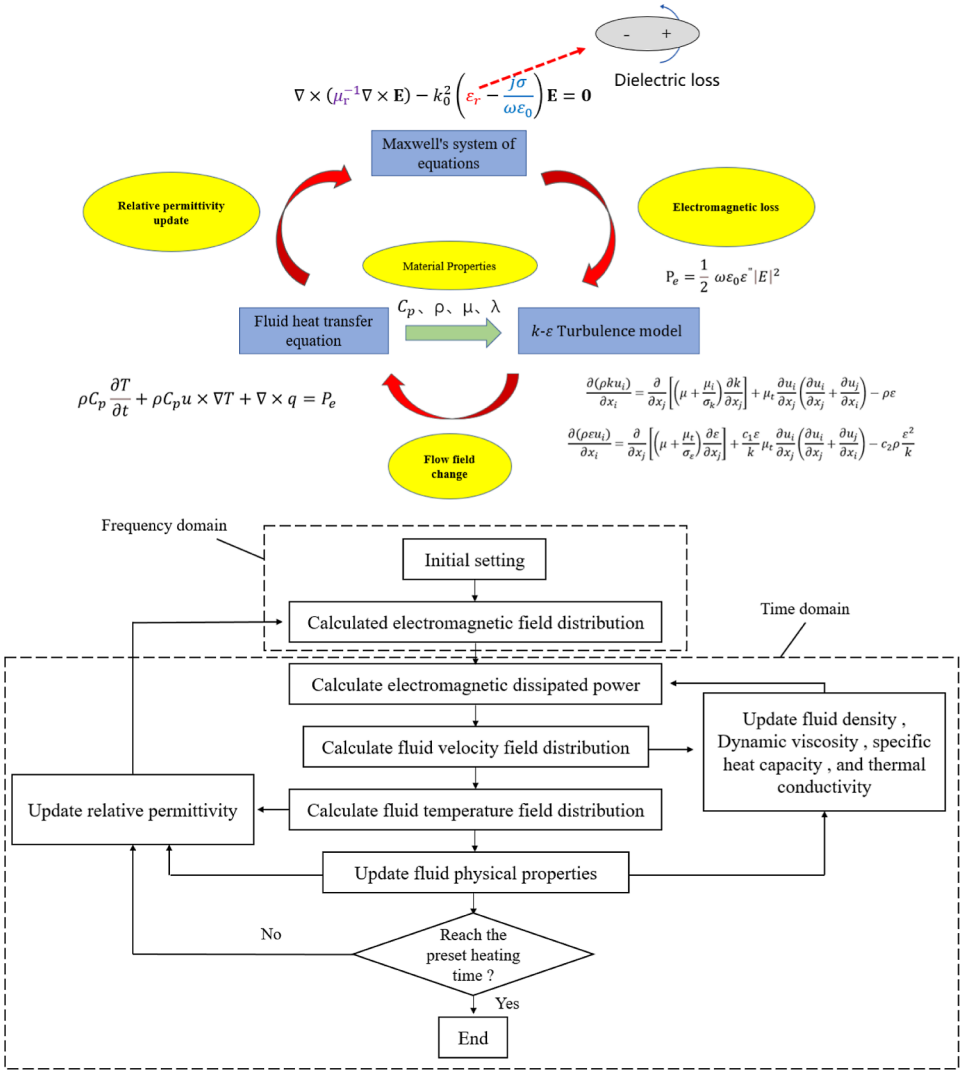

Figure 2. Flowchart of simulation calculation.

https://doi.org/10.1021/acsomega.3c04679
ACS Omega 2023, 8, 42367−42378

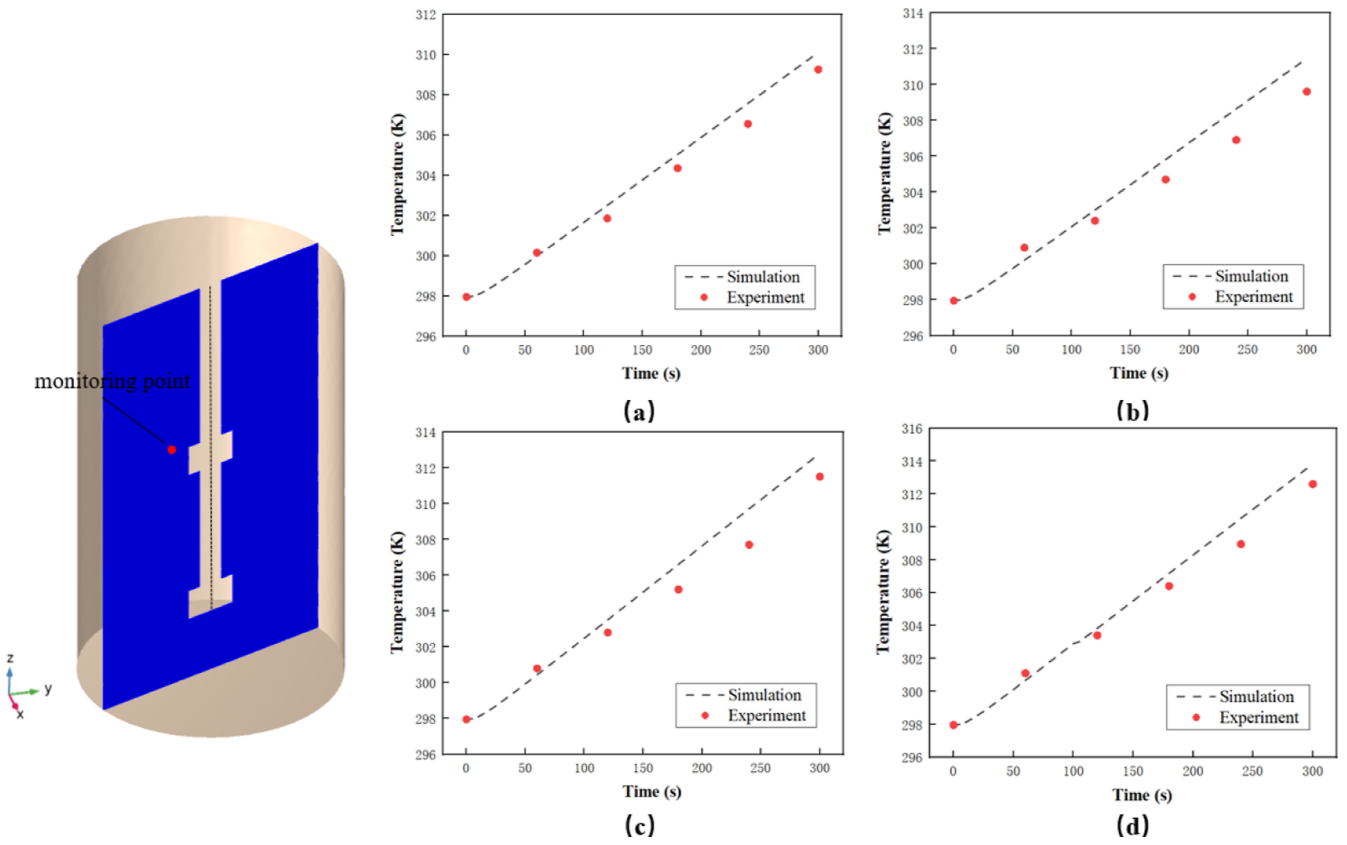

Figure 4. Temperature at the temperature measurement point obtained by simulation and experiment [microwave power 450 (a), 500 (b), 550 (c), 600 W (d)].

the digital timer was activated. After the reaction occurred for a period of time, the mixer and timer were stopped simultaneously. The reaction solution was filtered with an SHZ-D (III) vacuum pump. The manganese content of the filtrate was titrated with $(NH_4)_2Fe(SO_4)_2$ solution. For the accuracy of the data, two replicate tests were performed under the same conditions.

In the leaching process of soft manganese ore, the material of the rigid stirring paddle and stirring rod used is PTFE (Polytetrafluoroethylene), the flexible stirring paddle is a thin sheet of PTFE, and the rigid stirring paddle and the flexible stirring paddle are connected with a ring made of PTFE. The schematic diagram of the experimental system with the established 3D model can be found in Figure 1. In the experiments and simulations, the default input parameters are microwave power of 450 W (all microwave frequencies are 2.45 GHz), RF stirring paddle speed of 120 rpm, RF stirring paddle height from the bottom of 3 cm, rigid stirring paddle diameter from 2.5 cm, and flexible stirring paddle width from 1 cm. During the simulation calculations, in order to obtain a model that is easier to simulate, the mineral paddle reacted in the experiment is considered as an ideal fluid, and some important parameters are set by substituting functions considering the effect of temperature on the material parameters,[4] as shown in Table 1.

2.2. Modeling. The 3D geometry of the above experimental system is developed in commercial finite element software, COMSOL Multiphysics. The dimension of the calculation model can be found in Figure 1b.

The multiphysics field simulation of microwave heated fluid is calculated using Maxwell's equations, fluid flow equations, and heat conduction equations coupled with each other, and the distribution of electromagnetic field is calculated by solving Maxwell's waveform equations in the frequency domain[22]

$$\nabla \times \mu_r^{-1}(\nabla \times E) - k_0^2 \varepsilon_r E = 0 \tag{1}$$

In the calculation, the electromagnetic power absorbed by the microwave heated material is P_e, and P_e, as the heat source, is obtained from the following equation[23]

$$P_e = \frac{1}{2}\omega\varepsilon_0\varepsilon'' |E|^2 \tag{2}$$

The fluid flow state inside the reactor is judged to be in a turbulent state, so the simulation of this multiphysics coupled model uses the $k-\varepsilon$ model to calculate the fluid flow problem inside the reactor.[20]

The model uses the dynamic mesh in COMSOL Multiphysics to simulate the fluid flow inside the reactor. Continuity equation and momentum equation for turbulent time-averaged motion[19,23]

$$\frac{\partial u_i}{\partial x_i} = 0 \tag{3}$$

$$\frac{\partial (u_i u_j)}{\partial x_j} = -\frac{\partial p}{\partial x_i} + \frac{\mu}{\rho}\frac{\partial^2 u_i}{\partial x_i \partial x_j} - \frac{\partial (\overline{u_i' u_j'})}{\partial x_j} + f_i \tag{4}$$

Turbulent kinetic energy equations[24]

https://doi.org/10.1021/acsomega.3c04679
ACS Omega 2023, 8, 42367−42378

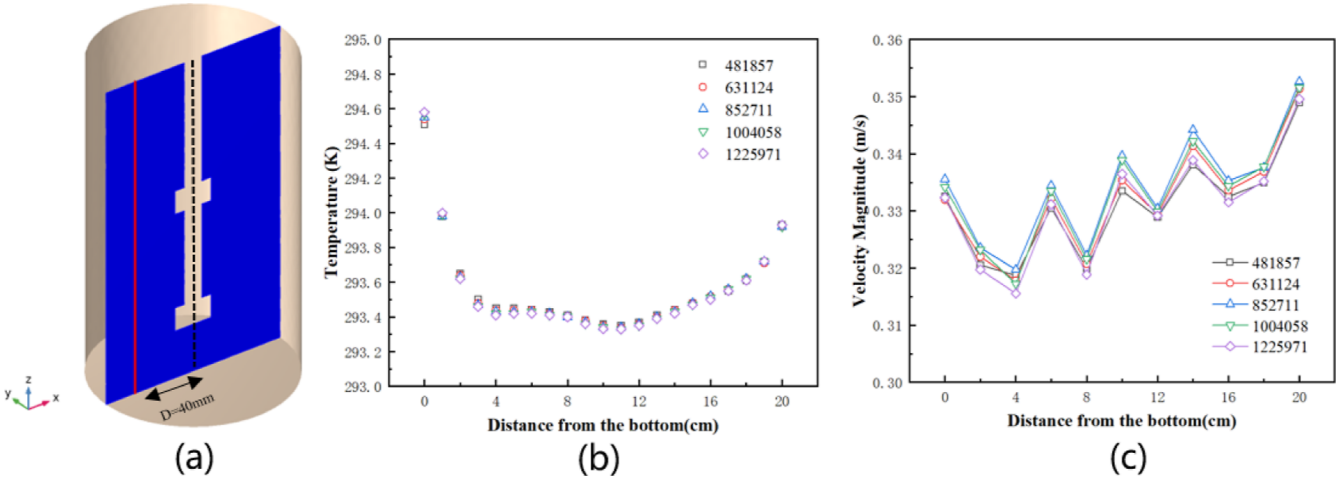

Figure 5. Grid-independent verification [diagram of monitoring surfaces and monitoring lines (a), temperature distribution (b), speed distribution (c)].

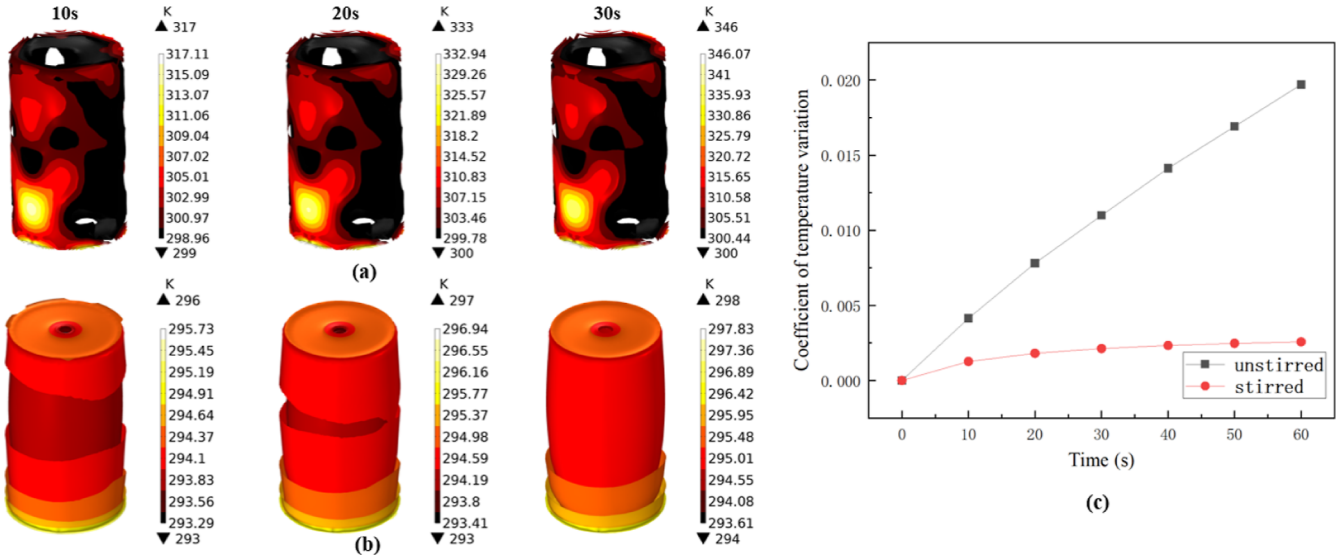

Figure 6. Temperature isosurface distribution without stirring (a), temperature isosurface distribution after stirring (b), and COV comparison (c).

$$\frac{\partial(\rho k u_i)}{\partial x_i} = \frac{\partial}{\partial x_j}\left[\left(\mu + \frac{\mu_i}{\sigma_k}\right)\frac{\partial k}{\partial x_j}\right] + \mu_t \frac{\partial u_i}{\partial x_j}\left(\frac{\partial u_i}{\partial x_j} + \frac{\partial u_j}{\partial x_i}\right) - \rho\varepsilon \tag{5}$$

$$\frac{\partial(\rho \varepsilon u_i)}{\partial x_i} = \frac{\partial}{\partial x_j}\left[\left(\mu + \frac{\mu_t}{\sigma_\varepsilon}\right)\frac{\partial \varepsilon}{\partial x_j}\right] + \frac{c_1 \varepsilon}{k}\mu_t \frac{\partial u_i}{\partial x_j}\left(\frac{\partial u_i}{\partial x_j} + \frac{\partial u_j}{\partial x_i}\right) - c_2 \rho \frac{\varepsilon^2}{k} \tag{6}$$

The relevant constants in the standard $k-\varepsilon$ equation are c_μ = 0.09, c_1 = 1.44, c_2 = 1.92, σ_k = 1, σ_ε = 1.3.

The heat transfer inside the reactor is mainly through fluid flow, and the equation used to describe fluid heat transfer is as follows

$$\rho C_p \frac{\partial T}{\partial t} + \rho C_p u \times \nabla T + \nabla \times q = P_e \tag{7}$$

The stepwise algorithm was adopted to simulate the heating process,[10] and the time step was set at 0.1 s. The fluid inside the reactor changed its physical properties with a change of temperature. In the COMSOL simulation process, the RF module and PARDISO direct solver are used to realize the calculation of electromagnetic field.[10] The fully coupled method of the MUMPS direct solver was adopted to solve the fluid temperature field and flow field distribution by the turbulence module, dynamic grid module, and fluid heat transfer module, respectively. The calculation program of the multiphysical field model is shown in Figure 2.

Considering the simulation of the turbulent flow model containing stirring paddles and the need for a more refined grid for the coupling calculation of fluid dynamics and electromagnetic heating, the grid of the material region is refined, and the grid cells of the material region are calibrated to fluid dynamics and are more refined (Figure 3b). Based on mesh convergence analysis, to ensure that when the number of grids is reduced by half, the change of any dependent variable does not exceed 1% of the total change,[24] the model uses 614,158 tetrahedral grids (Figure 3).

https://doi.org/10.1021/acsomega.3c04679
ACS Omega 2023, 8, 42367−42378

3. RESULTS AND DISCUSSION

3.1. Model Validation. The point temperature in the experiment was compared with the simulated point temperature (temperature point coordinates were $x = 0$, $y = -2$, $z = 11$) at different microwave power (microwave power was 450, 500, 550, 600 W, respectively). The stirring speed in the experiment was 120 rpm, and the microwave frequency was 2.45 GHz. The simulation results were more consistent with the measured results, but the simulated temperature was higher than the measured temperature. The deviations may be due to the use of assumed constant electrical and thermal parameters as well as the lag in temperature measurement. Comparing the simulated and experimental data, the average relative errors of the obtained point temperatures are 2.04, 3.17, 3.33, and 2.51%, respectively. In general, the measured temperature and simulated results match well, which verifies the validity of the model (Figure 4).

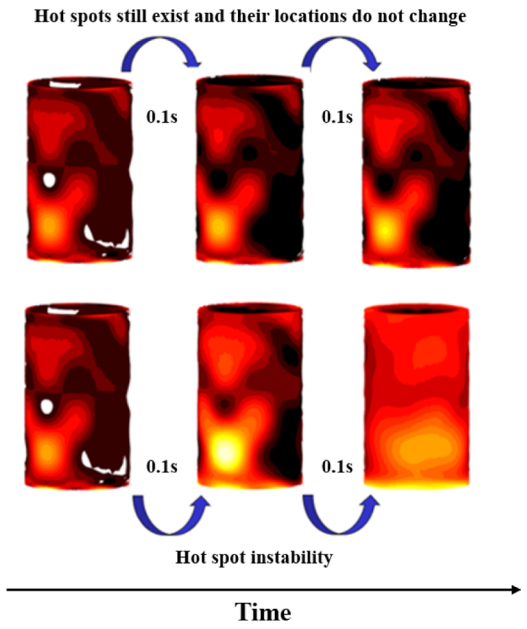

Figure 7. Hot spot destabilization schematic.

Local temperature distributions and velocity magnitude distributions are compared for microwave reactors with a total number of grid cells of 481,857, 631,124, 852,711, 1,004,058, and 1,225,971, respectively. The detection line is taken from a straight line with radial coordinate $x = -40$ mm and axial coordinate $z = 0-200$ mm in the xz plane in the stirring tank, and the temperature of the fluid at each point of the rigid−flexible combination stirring paddle on the monitoring line, as well as the distribution of the fluid velocity, is extracted by calculation, so as to analyze the influence of the number of grids on the simulation results.

The grid validation plot is shown in Figure 5. From the plot, it can be seen that when the number of grids is increased from 481,857 to 1,225,971, the overlap of temperature distribution curves and velocity distribution curves under five different grid numbers is higher, and this validation experiment can be considered to show that the number of grids delineated has less influence on the calculation results. Combined with the grid validation graph, 631,124 and 1,225,971 have almost double the difference in the number of grids, but the temperature and velocity distribution curves in the detection line have the highest degree of coincidence. In order to ensure

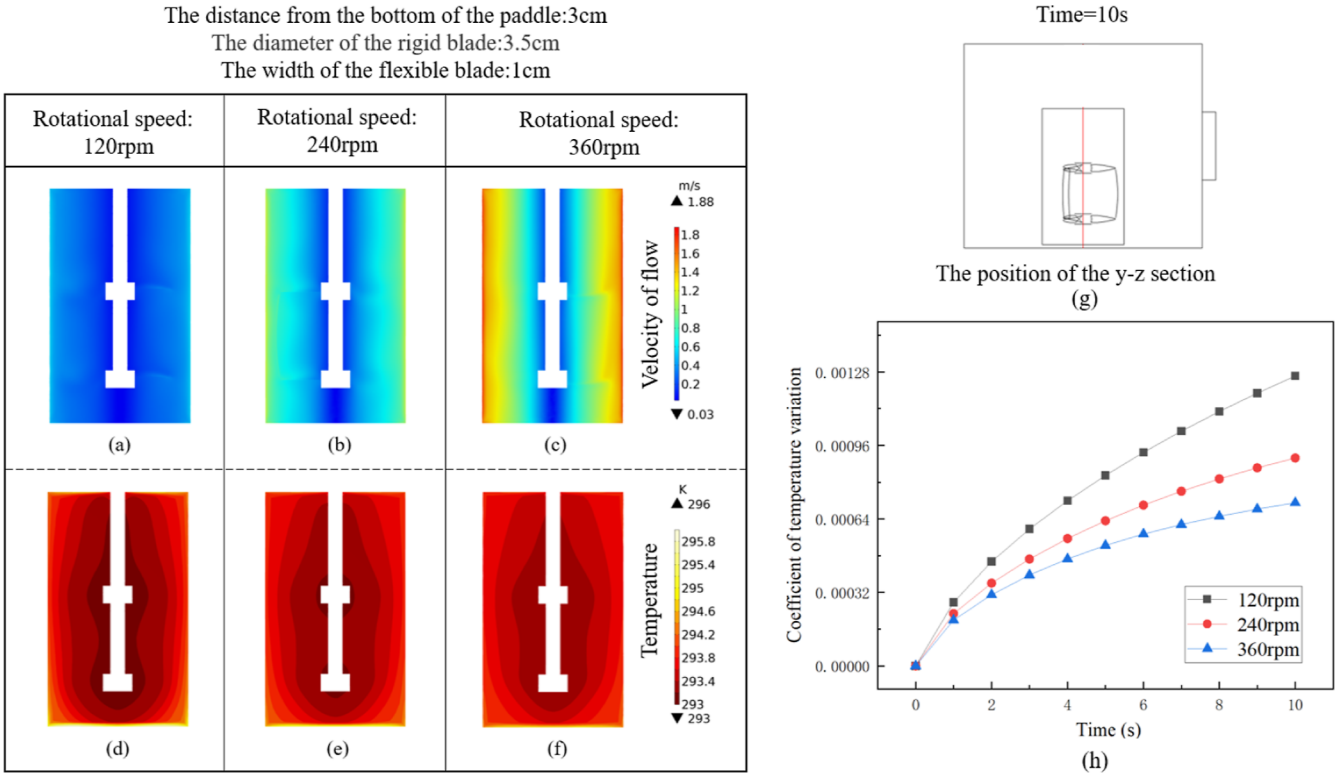

Figure 8. Comparison graphs of velocity field distribution (a−c), temperature field distribution (d−f), and COV at $y-z$ cross-section at different rotational speeds (h) and the location of $y-z$ cross-section (g).

https://doi.org/10.1021/acsomega.3c04679
ACS Omega 2023, 8, 42367−42378

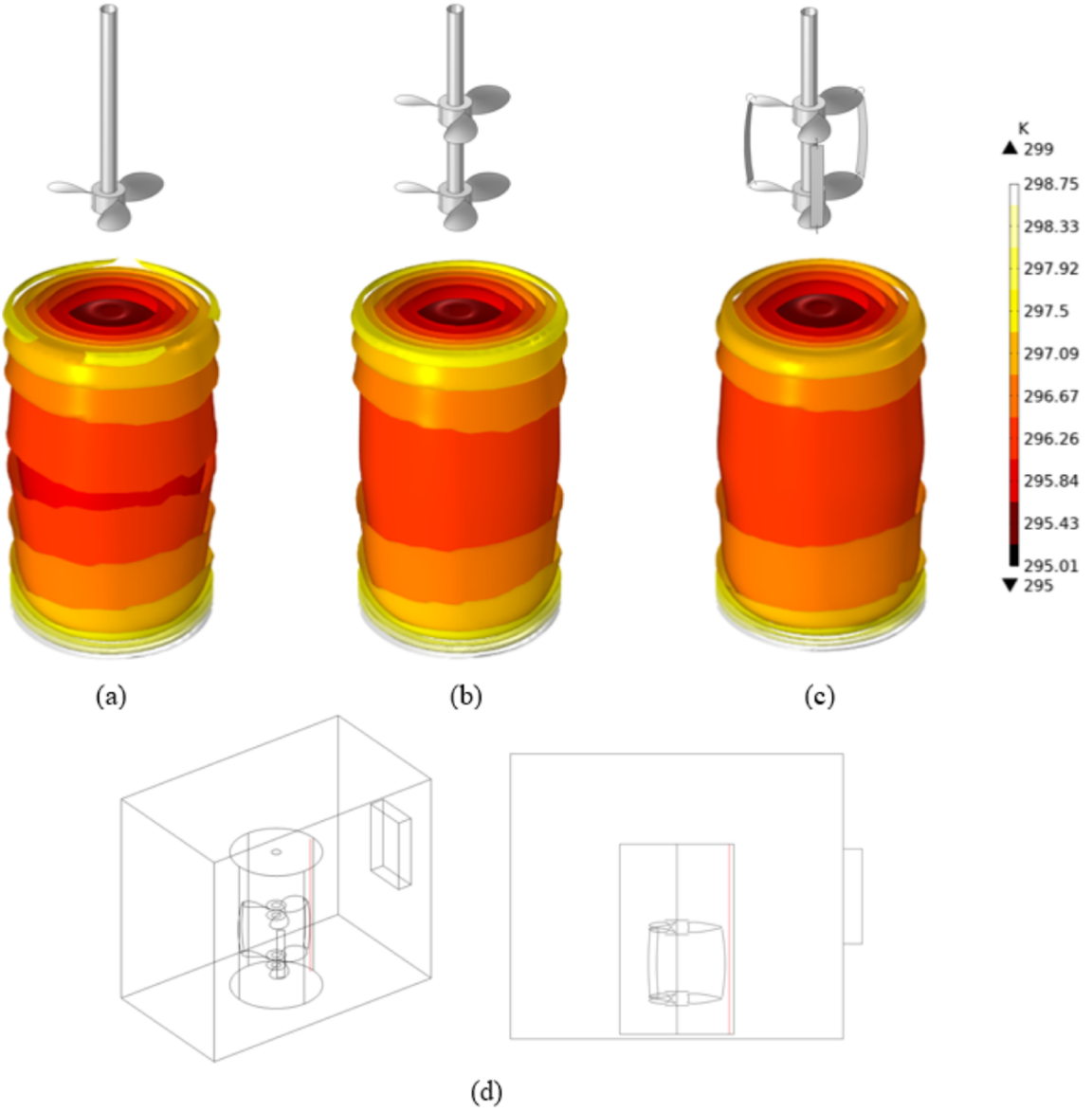

Figure 9. Temperature profile distribution of conventional single-layer stirrer (a), conventional double-layer stirrer (b), and RF stirrer (c) and, the position taken by the 3D intercept line (d).

high accuracy and simplify the calculation, 631,124 meshes are used for all subsequent calculations.

3.2. Effect of Stirring on Fluid Heating Uniformity. Comparing the temperature distribution in the reactor without stirring and the stirring paddle speed of 120 rpm, as shown in Figure 6. The temperature equivalence surface in the unstirred reactor was not uniformly distributed, and there were hot spots (i.e., heat concentration areas), which were always present and did not change position; the hot spots in the reactor with a stirring speed of 120 rpm were shifted, and the heat in the hot spot area was transferred through the fluid, so that the heat was more uniformly distributed in the reactor and the microwave heating effect was greatly improved (Figure 7).

To quantify the homogeneity of the microwave heated fluid, the temperature coefficient of variation of the fluid in the reactor is compared (Figure 6c), stirring can effectively reduce the temperature coefficient of variation of the fluid in the reactor and enhance the homogeneity of the microwave heated fluid.[17]

In the velocity cloud plot distribution of the $y-z$ cross-section (the x-coordinate of the $y-z$ section is 0) at different rotational speeds (Figure 8g), the overall fluid flow velocity in the reactor increases with the increase of rotational speed, but the distribution of fluid flow velocity is more consistent, with the fastest fluid flow velocity near the reactor wall and then decreasing inward (Figure 8a–c); considering that the increase in rotational speed and the overall acceleration of the fluid flow rate in the reactor facilitates heat transfer, the higher the rotational speed the better the heat transfer between the fluids. Therefore, the temperature distribution at different rotational speeds was also explored, and it was found that the more uniform the temperature equivalence surface on the $y-z$ cross section with the increase of the stirring paddle speed, the "stratification" of the temperature equivalence surface was reduced, and the heating uniformity was improved (Figure 8d–f). The temperature coefficient of variation of the fluid in the reactor can also be seen in the comparison chart (Figure 8h), the increase in speed can effectively reduce the

https://doi.org/10.1021/acsomega.3c04679
ACS Omega 2023, 8, 42367−42378

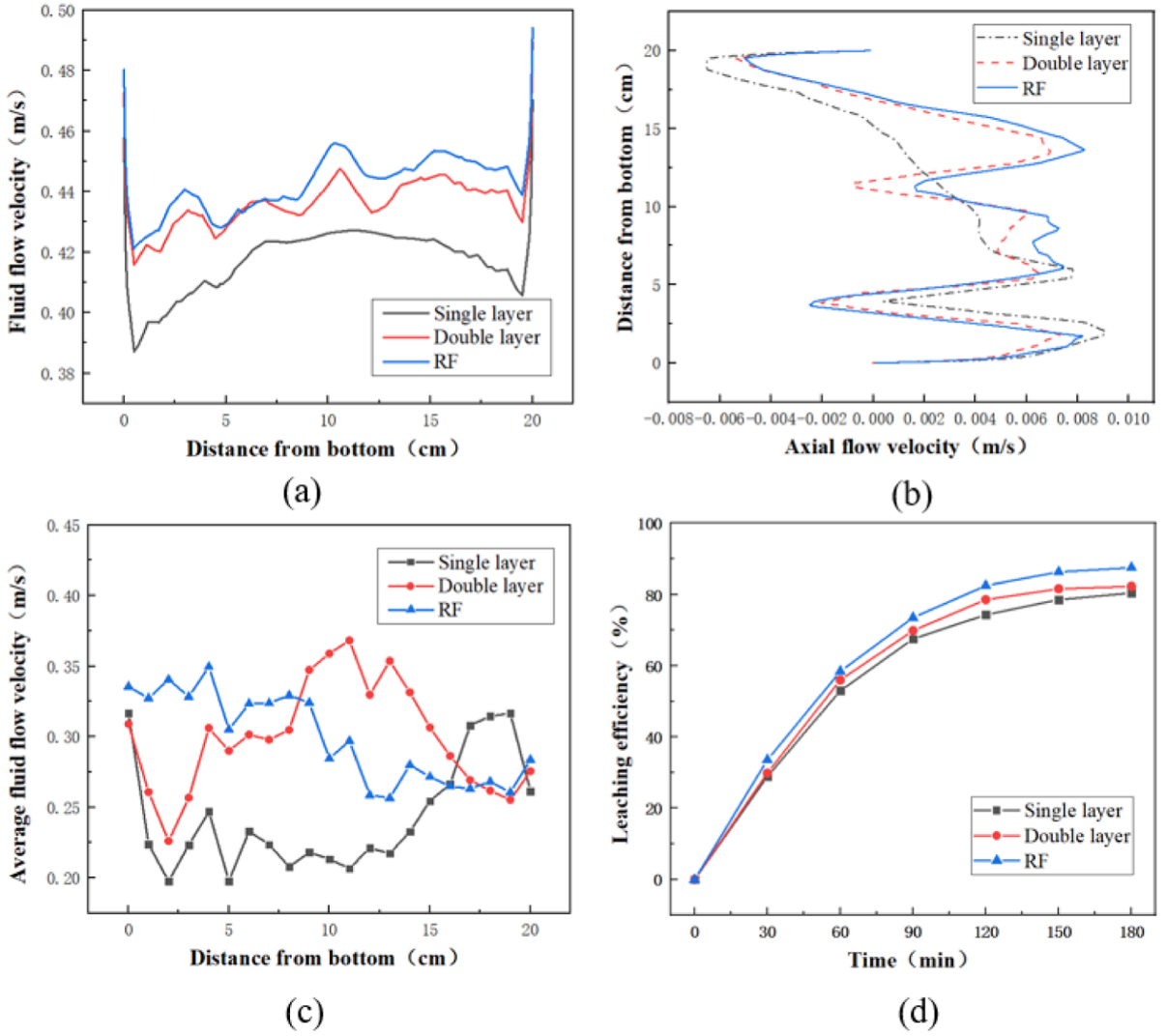

Figure 10. Fluid flow velocity (a) and axial flow velocity (b) at the 3D intercept line, fluid flow velocity (c), and soft manganese ore leaching rate (d) in the reactor for different stirring paddles.

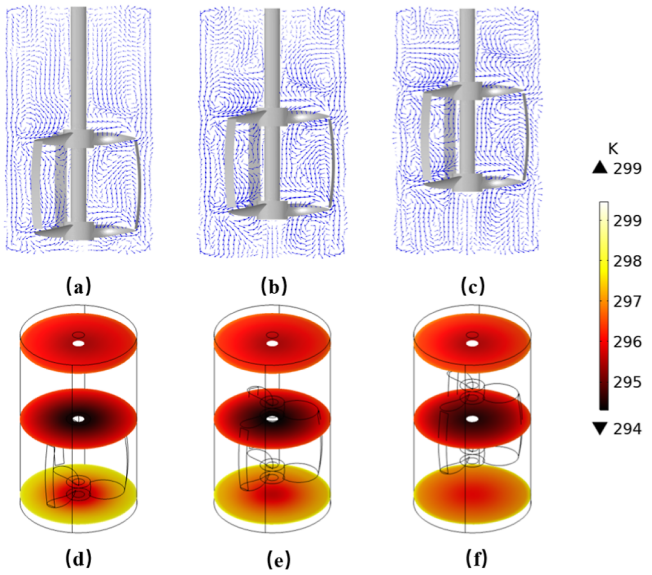

Figure 11. Flow field structure (a–c) and temperature field distribution (d–f) at different off-bottom heights.

temperature coefficient of variation of the fluid, which can improve the effect of microwave heating fluid.

3.3. Comparison with Conventional Paddle Type.

With the microwave heating process and rotation of the stirring paddle, the temperature distribution in the reactor of different paddle types varied after 60 s of simulated microwave heating (Figure 9). Among them, there are more temperature equivalence surfaces in the traditional single-layer stirred paddle reactor and the traditional double-layer stirred paddle reactor, and the phenomenon of "layering" of temperature equivalence surfaces appears in the figure, which indicates that the temperature distribution in the reactor is less uniform in space. In contrast, the temperature distribution in the RF stirred paddle reactor is more uniform than the above two traditional paddle types, especially near the wall, the RF stirred paddle reactor has fewer temperature equivalent surfaces.

For this phenomenon, a three-dimensional intercept line (consisting of two points with coordinates $x = 5.5$, $y = 0$, $z = 20$, and $x = 5.5$, $y = 0$, $z = 0$, Figure 9d) was taken near the wall of the reactor to investigate the effect of the flexible paddle on improving the microwave heating fluid. From the three-dimensional intercept of the fluid flow velocity graph, it can be seen that the participation of the flexible blade in the RF

https://doi.org/10.1021/acsomega.3c04679
ACS Omega 2023, 8, 42367−42378

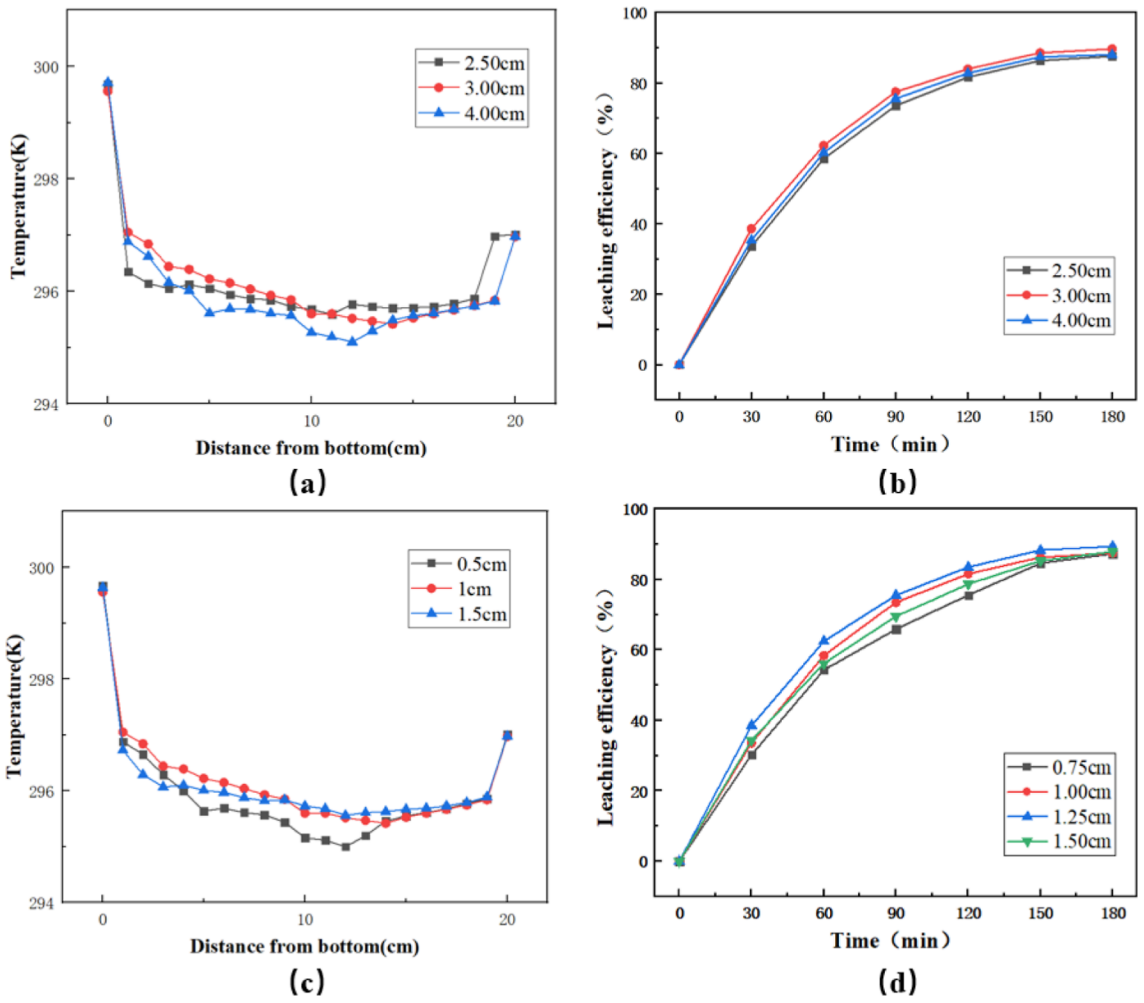

Figure 12. Comparison of temperature distribution (a) and leaching rate of soft manganese ore (b) for different rigid paddle diameters and temperature distribution (c) and leaching rate of soft manganese ore (d) for different flexible paddle widths.

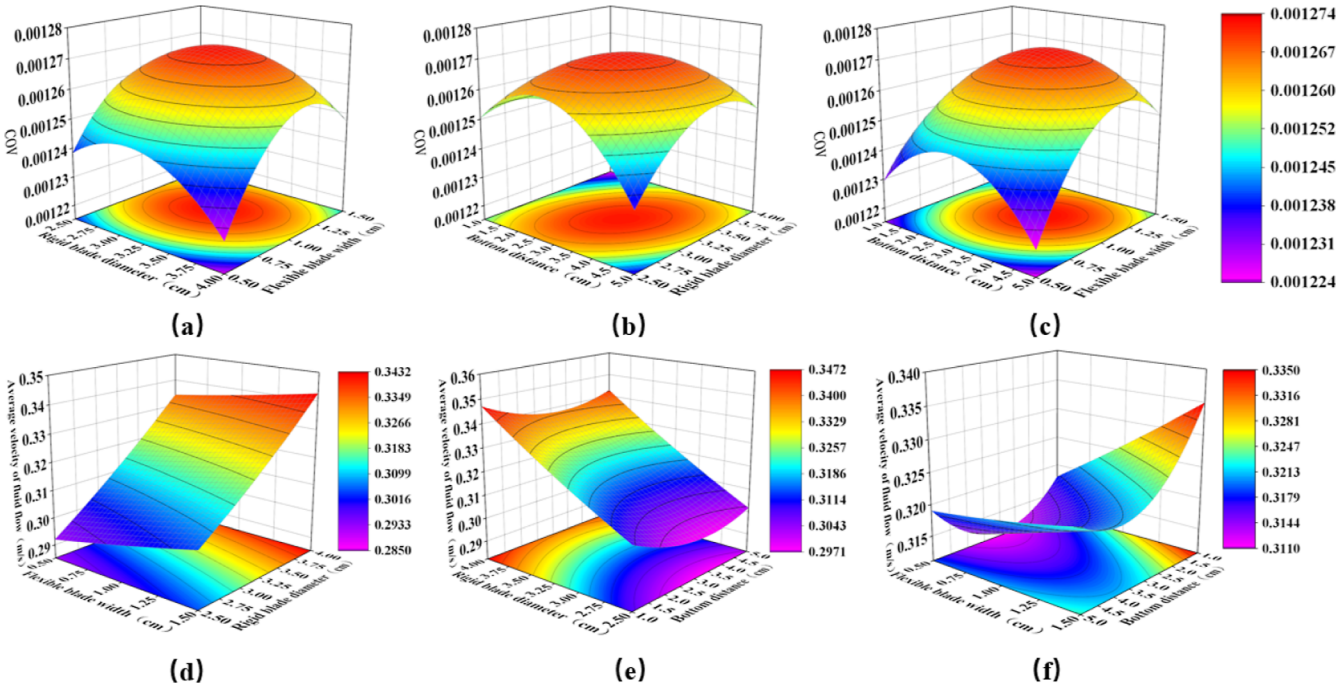

Figure 13. Response surface with COV as the response value (a−c) and response surface with average temperature as the response value (d−f).

https://doi.org/10.1021/acsomega.3c04679
ACS Omega 2023, 8, 42367−42378

stirring paddle plays a role in shearing the fluid and pushing the fluid axial movement (Figure 10b), making the fluid flow velocity at the three-dimensional intercept faster than other paddle types (Figure 10a), which accelerates the heat transfer and is conducive to promoting the uniform temperature distribution; compared with the traditional single-layer and double-layer paddles, RF stirring paddle can make the fluid flow rate in the reactor more balanced in space, especially improving the flow rate of the fluid at the bottom, which is conducive to strengthening the fluid flow in the higher temperature basin at the bottom of the reactor, enhancing the heat transfer of the fluid, and improving the uniformity of microwave heating (Figure 10c).

According to the preliminary research and experiments, temperature has a great influence on the leaching process of soft manganese ore, especially on the leaching rate.[4] The simulation results show that the combined rigid and flexible stirring paddle can make the temperature distribution more uniform and the fluid flow rate in the reactor more spatially even, both of which are beneficial to the leaching of soft manganese ore.

Combined experiments revealed that under the conditions of microwave power of 450 W (microwave frequency of 2.45 GHz) and RF stirring paddle rotation speed of 120 rpm, the leaching rate was increased by 7.08 and 5.22%, respectively, compared with the conventional single- and double-layer stirring paddles (Figure 10d), which showed that the combined RF stirring paddle can effectively improve the leaching rate and leaching efficiency with enhanced uniformity of the microwave heating solution.

3.4. Optimal Mixing Paddle Parameters. The flow field structure diagram and temperature field distribution of the RF stirring paddle at different off-bottom distance positions (Figure 11) were obtained by simulating the heating time of 60 s. The number of vortices generated by the RF stirring paddle is the same at different off-bottom distance positions (different distances h from the bottom are 1, 3, 5 cm), but the position distribution is not consistent. The fluid is subjected to rigid paddle lift and centrifugal force, and flows upward diagonally along the rigid paddle, and when it hits the wall of the reactor, the fluid continues to flow upward until it reaches the point where the fluid has no upward velocity, when the fluid starts to fall back down to form vortices; at the same time, the flexible paddle also continuously shears and disturbs the fluid between the two layers of rigid paddles during the stirring process, forming small vortices (Figure 11a−c).

The installation position of the stirring paddle is too close to the bottom of the reactor, but it is not conducive to fluid heat transfer at the bottom of the reactor. The stirring paddle is placed too low, which hinders fluid heat transfer at the bottom of the reactor. The analysis combined with the flow field structure is due to the vortex near the lower paddle, and the distance between the paddle and the bottom of the reactor is too close, resulting in poor heat transfer between the lower stirring paddle and the bottom wall of the reactor, and excessive heat concentration at the bottom of the reactor, which affects the uniformity of the heated fluid (Figure 11d−f).

The effect of other parameters of the stirring paddle on the temperature field was explored and compared, and it was found that appropriately increasing the diameter of the rigid paddle and the width of the flexible paddle was favorable to the uniform distribution of temperature in the reactor. The main reason is that the increase of the rigid paddle diameter may make the mixing process more fluid by the paddle to promote the impact to the reaction kettle wall to form the reflux; with the increase of the width of the flexible paddle and thus more radial flow of the fluid did not increase the axial flow, so that the reaction kettle inside weakens the effect of the heat transfer of fluids. From the results of the leaching rate experiments, it can also be seen that an appropriate increase in the diameter of the rigid paddle and the width of the flexible paddle can improve the heating effect of the system, which is conducive to the leaching rate and leaching rate (Figure 12).

In addition to investigating the effect of RF stirring paddle parameters on microwave heating characteristics, a three-factor, three-level response surface test was designed using Design-Expert. The response values of COV and mean fluid flow velocity after 10 s of simulated microwave heating were used to analyze the off-bottom height, rigid paddle diameter, and flexible paddle width of the stirrer. The results of the response surface test were analyzed by ANOVA, and it was found that each factor of the RF stirrer had a significant effect on the COV and the mean fluid flow velocity (Figure 13). The larger and steeper the gradient of the curve of the response surface in the figure indicates the more significant effect of the factors on the COV or average fluid flow velocity; therefore, based on the response surface ANOVA and the curve plot, the stirring conditions for the best COV were obtained as follows: rigid paddle diameter of 3.96 cm, flexible paddle width of 1.43 cm, and distance from the bottom of 1.21 cm; the stirring conditions for the best average fluid flow velocity were obtained as follows: rigid paddle diameter of 3.79 cm, flexible paddle width of 1.38 cm, and distance from the bottom of 1.17 cm. The differences in the optimal parameters of the COV and average fluid flow velocity are mainly due to the uneven distribution of the heat area generated by the microwave heating fluid in the reactor.

4. CONCLUSIONS

The calculated results of the model are in good agreement with the experimental results, indicating that the model can be used as an effective method to analyze the heat and temperature distribution of the microwave-heated fluid. The stirring effect of the RF stirring paddle and the regulation of the stirring paddle speed can well avoid the uneven heating caused by the short penetration depth of the microwave and the hot spots and thermal runaway caused by the uneven distribution of the electromagnetic field. The RF stirring paddle compared with the traditional single- and double-layer stirring paddles, the shear and disturbance of the rigid paddle to the fluid can more effectively improve the temperature distribution of the fluid in the microwave heating process. In addition, moderately increasing the rigid paddle diameter and flexible paddle width can improve the heating effect of the system.

AUTHOR INFORMATION

Corresponding Author

Renlong Liu − *College of Chemistry and Chemical Engineering and State Key Laboratory of Coal Mine Disaster Dynamics and Control, Chongqing University, Chongqing 400044, China;* orcid.org/0009-0004-9591-9331; Email: lrl@cqu.edu.cn

https://doi.org/10.1021/acsomega.3c04679
ACS Omega 2023, 8, 42367−42378

Authors

Shujin Chen − *College of Chemistry and Chemical Engineering, Chongqing University, Chongqing 400044, China;* orcid.org/0009-0002-8574-6604

Shaodou Cen − *College of Chemistry and Chemical Engineering, Chongqing University, Chongqing 400044, China*

Changyuan Tao − *College of Chemistry and Chemical Engineering and State Key Laboratory of Coal Mine Disaster Dynamics and Control, Chongqing University, Chongqing 400044, China*

Shenghui Guo − *Faculty of Metallurgical and Energy Engineering, Kunming University of Science and Technology, Kunming 650093, PR China*

Guo Chen − *Faculty of Metallurgical and Energy Engineering, Kunming University of Science and Technology, Kunming 650093, PR China*

Complete contact information is available at: https://pubs.acs.org/10.1021/acsomega.3c04679

Notes

The authors declare no competing financial interest.

■ ACKNOWLEDGMENTS

This work was supported by the National Natural Science Foundation of China (no. U1802255).

■ NOMENCLATURE

T temperature (C)
E electric field (V/m)
K thermal conductivity (W/(m °C))
k turbulent kinetic energy
k_0 wave number in vacuum (rad/m)
C_p specific heat capacity (J/(kg °C))
P_e electromagnetic power dissipation (W)
p pressure (Pa)
u fluid velocity (m/s)
q heat flow density

■ GREEK SYMBOLS

ε turbulent dissipation rate
ε_r relative magnetic permeability
ε_0 vacuum permittivity, $8.854187817 \times 10^{-12}$ (F/m)
ε' real part of the relative effective permittivity
ε'' imaginary part of the relative effective permittivity
ρ density of the liquid (kg/m^3)
μ_t turbulent viscosity

■ REFERENCES

(1) (a) Liu, B.; Zhang, Y. B.; Lu, M. M.; Su, Z. J.; Li, G. H.; Jiang, T. Extraction and separation of manganese and iron from ferruginous manganese ores: A review. *Miner. Eng.* **2019**, *131*, 286−303. (b) Lin, S. D.; Li, K. Q.; Yang, Y.; Gao, L.; Omran, M.; Guo, S. H.; Chen, J.; Chen, G. Microwave-assisted method investigation for the selective and enhanced leaching of manganese from low-grade pyrolusite using pyrite as the reducing agent. *Chem. Eng. Process.* **2021**, *159*, 108209. (c) Li, K. Q.; Chen, J.; Peng, J. H.; Ruan, R.; Srinivasakannan, C.; Chen, G. Pilot-scale study on enhanced carbothermal reduction of low-grade pyrolusite using microwave heating. *Powder Technol.* **2020**, *360*, 846−854.

(2) Lin, S. D.; Gao, L.; Yang, Y.; Chen, J.; Guo, S. H.; Omran, M.; Chen, G. Efficiency and sustainable leaching process of manganese from pyrolusite-pyrite mixture in sulfuric acid systems enhanced by microwave heating. *Hydrometallurgy* **2020**, *198*, 105519.

(3) Li, K. Q.; Chen, G.; Li, X. T.; Peng, J. H.; Ruan, R.; Omran, M.; Chen, J. High-temperature dielectric properties and pyrolysis reduction characteristics of different biomass-pyrolusite mixtures in microwave field. *Bioresour. Technol.* **2019**, *294*, 122217.

(4) Li, K. Q.; Chen, J.; Chen, G.; Peng, J. H.; Ruan, R.; Srinivasakannan, C. Microwave dielectric properties and thermo-chemical characteristics of the mixtures of walnut shell and manganese ore. *Bioresour. Technol.* **2019**, *286*, 121381.

(5) Li, K. Q.; Jiang, Q.; Chen, G.; Gao, L.; Peng, J. H.; Chen, Q.; Koppala, S.; Omran, M.; Chen, J. Kinetics characteristics and microwave reduction behavior of walnut shell-pyrolusite blends. *Bioresour. Technol.* **2021**, *319*, 124172.

(6) Ismail, A. A.; Ali, E. A.; Ahmed, M. S.; Ibrahim, A.; Ahmed, M. S. A comparative study on acid leaching of low grade manganese ore using some industrial wastes as reductants. *Can. J. Chem. Eng.* **2004**, *82* (6), 1296−1300.

(7) (a) Acharya, C.; Kar, R. N.; Sukla, L. B. Studies on reaction mechanism of bioleaching of manganese ore. *Miner. Eng.* **2003**, *16* (10), 1027−1030. (b) Vracar, R. Z.; Cerovic, K. P. Manganese leaching in the FeS2-MnO2-O-2-H2O system at high temperature in an autoclave. *Hydrometallurgy* **2000**, *55* (1), 79−92.

(8) (a) Jones, D. A.; Lelyveld, T. P.; Mavrofidis, S. D.; Kingman, S. W.; Miles, N. J. Microwave heating applications in environmental engineering—a review. *Resour., Conserv. Recycl.* **2002**, *34* (2), 75−90. (b) Kappe, C. O. Controlled microwave heating in modern organic synthesis. *Angew. Chem., Int. Ed.* **2004**, *43* (46), 6250−6284. (c) Ching Lau, C.; Bayazit, M. K.; Reardon, P. J. T.; Tang, J. Microwave Intensified Synthesis: Batch and Flow Chemistry. *Chem. Rec.* **2019**, *19* (1), 172−187.

(9) Motasemi, F.; Ani, F. N. A review on microwave-assisted production of biodiesel. *Renewable Sustainable Energy Rev.* **2012**, *16* (7), 4719−4733.

(10) Arpia, A. A.; Chen, W.-H.; Lam, S. S.; Rousset, P.; de Luna, M. D. G. Sustainable biofuel and bioenergy production from biomass waste residues using microwave-assisted heating: A comprehensive review. *Chem. Eng. J.* **2021**, *403*, 126233.

(11) (a) Li, K.; Chen, J.; Peng, J.; Omran, M.; Chen, G. Efficient improvement for dissociation behavior and thermal decomposition of manganese ore by microwave calcination. *J. Cleaner Prod.* **2020**, *260*, 121074. (b) Li, K.; Chen, J.; Penga, J.; Ruand, R.; Srinivasakannan, C.; Chen, G. Pilot-scale study on enhanced carbothermal reduction of low-grade pyrolusite using microwave heating. *Powder Technol.* **2020**, *360*, 846−854.

(12) Ye, Q. X.; Zhu, H. B.; Zhang, L. B.; Liu, P.; Chen, G.; Peng, J. H. Carbothermal reduction of low-grade pyrolusite by microwave heating. *RSC Adv.* **2014**, *4* (102), 58164−58170.

(13) (a) Vadivambal, R.; Jayas, D. S. Non-uniform Temperature Distribution During Microwave Heating of Food Materials-A Review. *Food Bioprocess Technol.* **2010**, *3* (2), 161−171. (b) Horikoshi, S.; Osawa, A.; Abe, M.; Serpone, N. On the Generation of Hot-Spots by Microwave Electric and Magnetic Fields and Their Impact on a Microwave-Assisted Heterogeneous Reaction in the Presence of Metallic Pd Nanoparticles on an Activated Carbon Support. *J. Phys. Chem. C* **2011**, *115* (46), 23030−23035.

(14) Santos, T.; Valente, M. A.; Monteiro, J.; Sousa, J.; Costa, L. C. Electromagnetic and thermal history during microwave heating. *Appl. Therm. Eng.* **2011**, *31* (16), 3255−3261.

(15) Meng, Q.; Lan, J.; Hong, T.; Zhu, H. Effect of the rotating metal patch on microwave heating uniformity. *J. Microw. Power Electromagn. Energy* **2018**, *52* (2), 94−108.

(16) Sebera, V.; Nasswettrova, A.; Nikl, K. Finite Element Analysis of Mode Stirrer Impact on Electric Field Uniformity in a Microwave Applicator. *Drying Technol.* **2012**, *30* (13), 1388−1396.

(17) Geedipalli, S. S. R.; Rakesh, V.; Datta, A. K. Modeling the heating uniformity contributed by a rotating turntable in microwave ovens. *J. Food Eng.* **2007**, *82* (3), 359−368.

(18) Ye, J.-H.; Zhu, H.-C.; Liao, Y.-H.; Zhou, Y.-P.; Huang, K.-M. Implicit Function and Level Set Methods for Computation of Moving Elements During Microwave Heating. *IEEE Trans. Microwave Theory Tech.* **2017**, *65* (12), 4773−4784.
(19) Gu, D.; Liu, Z.; Qiu, F.; Li, J.; Tao, C.; Wang, Y. Design of impeller blades for efficient homogeneity of solid-liquid suspension in a stirred tank reactor. *Adv. Powder Technol.* **2017**, *28* (10), 2514−2523.
(20) Gu, D. Y.; Liu, Z. H.; Xie, Z. M.; Li, J.; Tao, C. Y.; Wang, Y. D. Numerical simulation of solid-liquid suspension in a stirred tank with a dual punched rigid-flexible impeller. *Adv. Powder Technol.* **2017**, *28* (10), 2723−2734.
(21) Walkiewicz, J. W.; Kazonich, G.; McGill, S. L. Microwave Heating Characteristics of Selected Minerals and Compounds. *Min., Metall., Explor.* **1988**, *5*, 39−42.
(22) (a) Huang, K.-m.; Liao, Y.-h. Transient Power Loss Density of Electromagnetic Pulse in Debye Media. *IEEE Trans. Microwave Theory Tech.* **2015**, *63* (1), 135−140. (b) Hong, Y.-d.; Lin, B.-q.; Li, H.; Dai, H.-m.; Zhu, C.-j.; Yao, H. Three-dimensional simulation of microwave heating coal sample with varying parameters. *Appl. Therm. Eng.* **2016**, *93*, 1145−1154.
(23) Tamburini, A.; Cipollina, A.; Micale, G.; Brucato, A.; Ciofalo, M. CFD simulations of dense solid-liquid suspensions in baffled stirred tanks: Prediction of the minimum impeller speed for complete suspension. *Chem. Eng. J.* **2012**, *193*−*194*, 234−255.
(24) Gulati, T.; Zhu, H.; Datta, A. K. Coupled electromagnetics, multiphase transport and large deformation model for microwave drying. *Chem. Eng. Sci.* **2016**, *156*, 206−228.

https://doi.org/10.1021/acsomega.3c04679
ACS Omega 2023, 8, 42367−42378